Rev. Adv. Mater. Sci. 48 (2017) 13-24

STRENGTHENING OF METALS THROUGH SEVERE PLASTIC DEFORMATION

Megumi Kawasaki[1,2], Han-Joo Lee[1], Jae-il Jang[1] and Terence G. Langdon[2,3]

[1] Division of Materials Science & Engineering, Hanyang University, Seoul 04763, South Korea
[2] Departments of Aerospace & Mechanical Engineering and Materials Science, University of Southern California, Los Angeles, CA 90089-1453, U.S.A.
[3] Materials Research Group, Faculty of Engineering and the Environment, University of Southampton, Southampton SO17 1BJ, U.K.

Received: November 23, 2016

Abstract. The processing of bulk metals through the application of severe plastic deformation (SPD) provides an opportunity for achieving excellent grain refinement to the submicrometer or even the nanometer range. These SPD procedures produce materials exhibiting improved mechanical properties including very high strength. This report describes recent results demonstrating the strengthening of conventional metallic alloys processed by high-pressure torsion (HPT). It shows also that exceptionally high strength may be achieved by synthesizing a metal matrix nano-composite using HPT to simultaneously process two different metal disks. Special emphasis is placed on the significance of grain refinement in producing strengthening by HPT.

1. INTRODUCTION

For all structural applications, the strength of a metal remains the pre-eminent property and the characteristic that most readily defines and differentiates different materials. In practice, the strength is dependent upon many separate properties such as the crystal structure and the presence of alloying elements in solid solution or as precipitates. Nevertheless, a major factor contributing to the overall strength of any selected metal is the grain size within the polycrystalline matrix. Within the thermally-activated regime at ambient and relatively low temperatures, where diffusion occurs very slowly, the yield stress of a metal, σ_y, is most readily defined in terms of the grain size, d, using the Hall-Petch relationship which is given by [1,2]

$$\sigma_y = \sigma_0 + k_y d^{-\frac{1}{2}}, \quad (1)$$

where σ_0 is the lattice friction stress and k_y is a constant of yielding. It follows from this relationship that the strength of a metal increases with decreasing grain size and therefore high strength is achieved most readily by performing thermo-mechanical treatments to reduce the grain size to the smallest possible level. There are now many reports documenting and supporting Eq. (1) in a very wide range of metals [3,4].

The importance of grain size, and the significance of thermo-mechanical treatments, is well-known in industrial practice but generally these treatments cannot reduce the grain size to a level smaller than a few micrometers. This situation changed more

Corresponding author: Terence G. Langdon: e-mail: langdon@usc.edu

than two decades ago with the demonstration that exceptional grain refinement may be achieved, even to the nanometer level, by processing metals through the imposition of severe plastic deformation (SPD) using techniques in which very high strains are imparted to the metal but without incurring any significant changes in the overall dimensions of the work-pieces [5]. Several different SPD processing techniques are now available but the two procedures receiving the most attention are equal-channel angular pressing (ECAP) [6] and high-pressure torsion (HPT) [7]. Comparing these two techniques, it is now established that HPT is the most effective because it produces the smallest grain sizes [8,9] and also it introduces, by comparison with ECAP, a higher fraction of grain boundaries having high angles of misorientation [10].

An inherent difficulty in HPT processing is that it entails the use of a thin disk and the equivalent strain, ε_{eq}, then varies across the disk through a relationship of the form [11]

$$\varepsilon_{eq} = \frac{2\pi Nr}{h\sqrt{3}}, \qquad (2)$$

where N is the number of revolutions in torsional straining, r is the radius of the disk and h is the height (or thickness) of the disk. This means that care must be taken examining the grain size and the strength across each HPT disk and in practice the strength is most readily evaluated by measuring the micro-hardness at selected positions within the disk diameter.

Professor Ilya Ovid'ko has made important contributions to our understanding of the properties of bulk nanocrystalline materials and accordingly, in honor of his 55th birthday, this paper is designed to examine typical measurements of strength in several different metallic systems. Initial attention is given to the strengthening of conventional metallic alloys through SPD processing but then recent results are described where it is possible to achieve exceptionally high strength, and the development of a metal matrix nano-composite, through the simultaneous HPT processing of disks of two different metals.

2. STRENGTHENING OF CONVENTIONAL METALS BY HPT PROCESSING

There are now a large number of separate reports describing the application of HPT processing to simple metallic systems. In this section, attention will be devoted to two typical metals, an Al-3% Mg solid solution alloy and a commercial magnesium ZK60 (Mg-5.5% Zn-0.5% Zr) alloy as representative of f.c.c. and h.c.p. materials, respectively.

2.1. Al-3% Mg alloy

Experiments were conducted using an Al-3% Mg alloy containing small amounts (<0.003%) of Si and Fe impurities. A billet with a diameter of 10 mm was annealed at 773 K for 1 hour to remove any residual stress so that an average grain size of $d \approx 830$ μm was obtained in the initial condition. The billet was sliced and polished to prepare disks having final thicknesses of ~0.83 mm. These disks were then processed by HPT at room temperature (RT) under quasi-constrained conditions [12] using a compressive pressure of 6.0 GPa and a speed of anvil rotation of 1 rpm. A set of disks was processed by HPT for total rotations, N, of 1/4, 1/2, 3/4, 1, 2, 5 and 10 turns.

The HPT-processed disks of the Al-3% Mg alloy were examined to record the Vickers microhardness values along the disk diameters and the variation of hardness across each disk is shown in Fig. 1 where the lower dashed line denotes the hardness value of Hv ≈ 50 for the as-annealed sample prior to HPT [13]. It should be noted that a ratio of disk thickness to diameter of ~1/13 is one of the critical parameters for hardness consistency in the direction of the disk thickness [14] where the present HPT

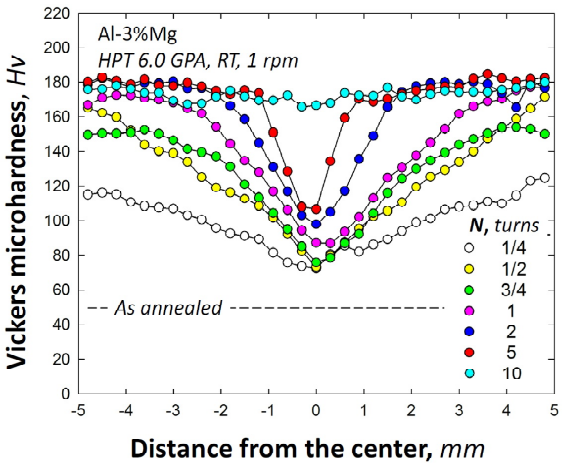

Fig. 1. Variation of Vickers microhardness values along diameters of Al-3% Mg alloy disks after HPT processing for different numbers of turns: the lower dashed line denotes the hardness value before HPT processing of $Hv \approx 50$ in the as-annealed condition, adapted from our work [13].

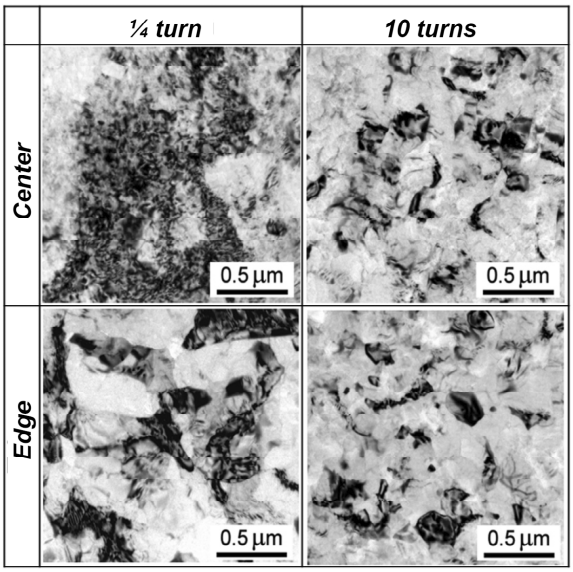

Fig. 2. Representative microstructures of Al-3% Mg disks processed by HPT for 1/4 turn on the left and for 10 turns on the right where all microstructures were taken on the plane parallel to the disk surface either near the center at $r \approx 0$ mm (upper row) or close to the edge at $r \approx 3.5$ mm (lower row), adapted from our work [13].

disks had ratios of ~1/12.5 and thus reasonably agree with this condition. Moreover, pure Al and Al alloys are typical materials showing reasonable hardness homogeneity through the height directions of the disks after HPT processing [15-17] and there is no influence of the measurement section within the disk thickness on the hardness variations along the disk diameters.

It is apparent that there are gradual changes towards homogeneity in hardness along the disk diameter. Specifically, the hardness values are higher even after 1/4 turn compared with the as-annealed condition and, except at 10 turns, all disks showed typical hardness behavior [18] in which the low hardness at the disk center increases towards the disk periphery with increasing equivalent strain by HPT as given in Eq. (1). Thus, HPT for 1/4 turn provided hardness values of ~75 and ~120 at the disk center and edge, respectively, and with increasing numbers of turns the hardness values both at the disk center and edge increase gradually and reach ~100 and ~180, respectively, after 5 turns. Thereafter, the hardness attained an essentially homogeneous hardness distribution with a high hardness of $Hv \approx 180$ throughout the disk diameter after 10 turns.

A concomitant microstructural evolution was observed by transmission electron microscopy (TEM) and representative microstructures are shown in Fig. 2 for the Al-3% Mg alloy after HPT for 1/4 turn in the left column and 10 turns in the right column where for each disk the microstructures in the upper and lower rows are for the centers at $r \approx 0$ mm and close to the edge at $r \approx 3.5$ mm, respectively [13].

Processing by HPT for 1/4 turn introduced a random non-cellular microstructure with many dislocations within coarse grains at the disk center whereas there are ill-defined boundaries forming insufficiently equiaxed grains due to significant numbers of dislocation introduced at the disk edge. With increasing torsional straining through 10 turns, the grain boundaries become well-defined and there are reasonably equiaxed ultrafine grains at the disk center which are comparable to the ultrafine microstructure at the disk edge. Therefore, a homogeneous ultrafine-grained (UFG) microstructure with average fine grains of ~180-190 nm was observed in the Al-3% Mg alloy after HPT for 10 turns. This refinement in grain size is consistent with numerous earlier reports of the grains sizes produced in various Al-Mg alloys after processing by HPT at RT [19-29].

The significant increase in hardness as shown in Fig. 1 is due to the dramatic reduction in grain size as demonstrated in Fig. 2 and it is explained by Hall-Petch strengthening as given in eq (1) when the relationship is reformulated in terms of hardness in the form

$$H = H_0 + k_H d^{-\frac{1}{2}}, \tag{3}$$

where H is the hardness and H_0 and K_H are the appropriate material constants associated with the hardness measurements. The validity of utilizing the modified Hall-Petch relationship in terms of Vickers microhardness was demonstrated in an earlier report using Al-3% Mg and Al-5.5% Mg-2.2% Li- 0.12% Zr alloys after processing by ECAP [30].

Accordingly, the grain refinement and the hardness increase was correlated by applying the relationship in Eq. (3) by plotting as a function of $d^{-1/2}$ for the Al-3% Mg alloy in an as-annealed condition without HPT and after HPT for 1/4, 1, 5 and 10 turns at the edge and center positions. This plot is shown in Fig. 3 [13] with additional datum points for the Al-3% Mg alloy after HPT for 5 and 10 turns followed by static annealing at 673 K for 1 h which gave consistent grain sizes of ~50-55 μm and a hardness of $Hv \approx 50$ and for a similar Al-3% Mg alloy processed either by ECAP [30] or HPT [21].

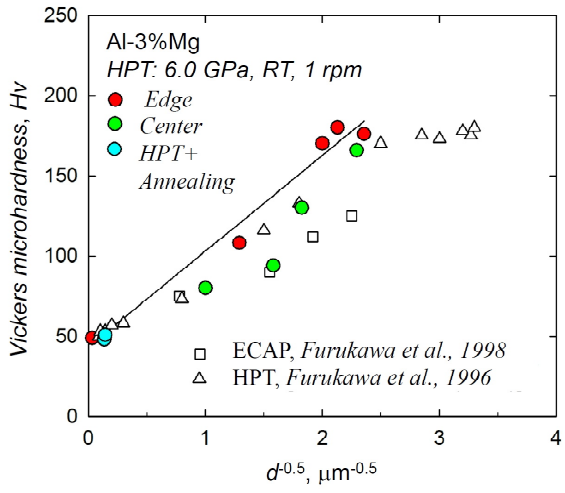

Fig. 3. Plot of Vickers microhardness as a function of $d^{-1/2}$ for the Al-3% Mg alloy in an initial state without HPT, after HPT for 1/4, 1, 5 and 10 turns at the center and edge positions and after HPT followed by static annealing at 673K for 1 h: for comparison purposes, additional datum points are included for a similar Al-3% Mg alloy processed either by ECAP [30] or HPT [21].

An excellent description of Hall-Petch strengthening through grain size reduction is provided in this analysis where there is a conventional linear relationship between hardness and the values of $d^{-1/2}$ for all sample conditions in the present Al-3% Mg alloy from coarse grain sizes in the initial condition and after processing and annealing to ultrafine grain sizes after HPT. In practice, all of the experimental points for this Al-Mg alloy lie close to a single trend line given by Eq. (3) with $H_0 \approx 59.7$ Hv and $K_H \approx 43.3$ Hv $\mu m^{-1/2}$. As seen in the reference datum points, a consistent relationship between hardness and grain size was reported on a similar alloy after ECAP and HPT with a recording of $H_0 \approx$ 46-47.5 Hv and $K_H \approx 35.0$-41.0 Hv $\mu m^{-1/2}$ [21,30]. Also, the consistent trend of Hall-Petch strengthening was reported in a dilute Al alloy with 1.5% Mg after HPT to a true logarithmic strain of 7 [19].

It should be noted that the saturated value of hardness in the present Al-3% Mg alloy is consistent with the alloy in the same composition after HPT under 5 GPa [21] but it is higher than the hardness value of ~130 after ECAP at RT [21,30] and this is due to the severe grain refinement during the HPT procedure which is more effective than processing by ECAP [31]. Moreover, recent reports showed that an Al-1% Mg alloy processed through HPT under 6.0 GPa after >3 turns demonstrated a hardness saturation with Hv ≈ 110 [28] and an Al-5% Mg alloy showed a homogeneous distribution of hardness with *Hv* ≈ 240 after HPT at 6.0 GPa for 10 turns [29]. Considered together with the present hardness experiments, these results lead to the conclusion that higher Mg contents lead to higher hardness values at the saturation stage after HPT and this trend continues up to at least 10% of Mg in the Al matrix after 10 turns by HPT [25].

2.2. ZK60 Magnesium alloy

A commercial-quality ZK60A magnesium alloy was prepared as a bar after extrusion with a diameter of 10 mm and a set of the disks was prepared in the same way as noted in the previous section. The ZK60A disks were then processed by HPT at RT under 6.0 GPa and a rotational speed of 1 rpm for total revolutions of 1/4, 1/2, 1, 2, 3 and 5 turns.

The microstructure at the edges of the ZK60A disks after HPT was examined using an optical microscope. Representative microstructures are shown in Fig. 4 for (a) the as-extruded condition and for the samples after HPT for (b) 1/4, (c) 1/2 and (d) 2 turns [32]. The as-extruded microstructure prior to HPT consisted of a bi-modal grain distribution with a fraction of >50% of coarse grains of ~25 μm surrounded by several small grains having sizes of ~4-5 μm as shown in Fig. 4a. A noticeable change is visible in the microstructure after HPT for 1/4 turn where the fraction and size of the coarse grains were reduced to ~35% and ~20 μm, respectively, and the fine grains were reduced to ~2-3 μm with an increased

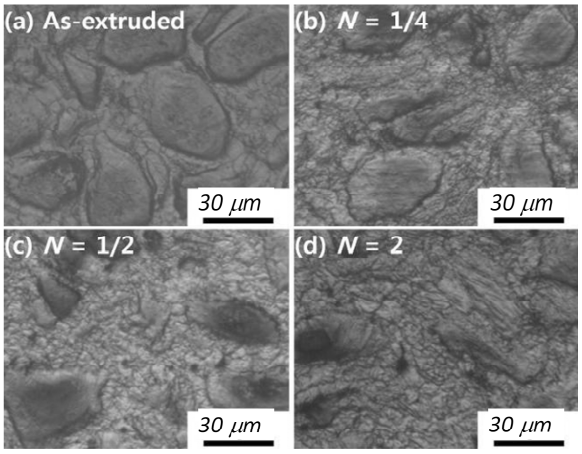

Fig. 4. Representative optical micrographs taken at the edges of ZK60A disks (a) in the as-extruded condition and after HPT for (b) 1/4, (c) 1/2 and (d) 2 turns, adapted from our work [32].

area fraction of ~65% as shown in Fig. 1b. After 1/2 turn in Fig. 1c, the coarse grain sizes remain the same size at ~20 μm with a slightly lower fraction than earlier whereas there are fine grains having an average size of ~1.0-1.5 μm with a high area fraction of ~75%. Thereafter, the microstructure remained constant with increasing torsional straining though 2 turns as shown in Fig. 1d. It is apparent that HPT processing introduces a reasonable level of microstructural saturation up to at least 2 turns in the ZK60A alloy.

The bi-modal grain size distribution observed in the alloy after HPT for 2 turns is in excellent agreement with a ZK60 alloy after ECAP at 473K [33] and after HPT at RT under 2.0 GPa for 5 turns [34]. This unique microstructural evolution in magnesium alloys is explained by the necklace-like dynamic recrystallization (DRX) where the concentration of deformation occurs across the new fine grains [35]. It is concluded that the saturated grain structure depends on the initial grain size, the size of the new grains and the magnitude of the imposed strain within magnesium alloys.

The evolution in microstructure produces appreciable changes in hardness so that the degree of microstructural evolution may be determined by the alternative approach of evaluating the variation of the measured microhardness values with increasing equivalent strain as calculated using Eq. (2). This approach was first demonstrated for an austenitic steel processed by HPT for increasing numbers of HPT revolutions under a pressure of 5.3 GPa [36] and a recent review used this approach for examining the hardness evolution in a large number of metals and alloys after processing by HPT [18]. Although a unique hardness behavior of materials was observed at a cryogenic temperature [37], there are currently three simple models of hardness evolution towards homogeneity that depend on the nature of microstructural recovery with increasing imposed strain within the material [38-40] together with an experimental factor of the homologous temperature of HPT processing [17,18].

Fig. 5 shows the alternative approach of plotting the variation of the measured microhardness values against the calculated equivalent strains using Eq. (2) for the ZK60A alloy after HPT for 1/4, 1/2, 1, 3 and 5 turns at 6.0 GPa where the lower dashed line denotes the hardness value of ~72 in the as-extruded condition and the error bars again denote the 95% confidence level [41]. This type of hardness behavior is the most common model of hardness evolution exhibiting a high hardness with increasing equivalent strain, thereby confirming the occurrence of strain hardening as in the present results for the ZK60A alloy and the Al-3% Mg alloy described in an earlier section. It is readily apparent that the hardness increases rapidly with increasing strain in the early stage of HPT but this trend becomes slower at equivalent strains around 20 and ultimately the hardness essentially saturates at a high *Hv* value of ~110 at high strains.

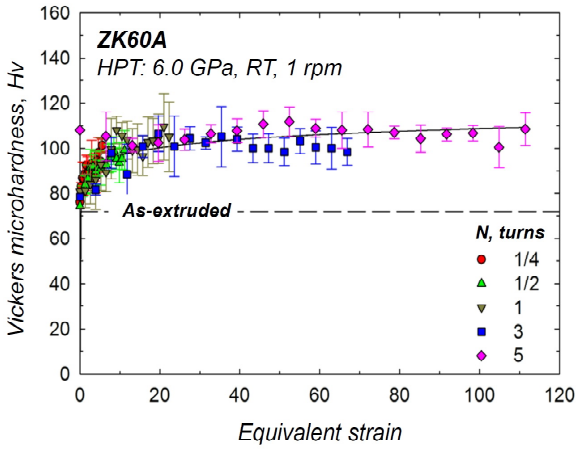

Fig. 5. Variation of the measured microhardness values with equivalent strain for the ZK60A alloy after HPT for 1/4, 1/2, 1, 3 and 5 turns under an applied pressure of 6.0 GPa: the lower dashed line denotes the microhardness value of Hv ≈ 72 in the as-extruded condition prior to HPT and the error bars show the 95% confidence level, adapted from our work [41].

For a better understanding of the significant level of strain hardening occurring in the early stage of plastic deformation, a further quantitative analysis was conducted on the HPT-processed ZK60A alloy in order to estimate the degree of strain hardening by calculating the hardenability exponent, η, which corresponds to the slope in a double-natural logarithmic plot of the Hv values versus equivalent strain. This approach was first demonstrated on a Ti-6% Al-4% V alloy after HPT from two different initial phase conditions and gave hardenability exponents of 0.031 and 0.052 [42].

The constructed double-natural logarithmic plot of the *Hv* values versus ε_{eq} is shown in Fig. 6 for the ZK60A alloy after HPT for up to 5 turns under 6.0 GPa in which the Hv values are taken from Fig. 5 up to $\varepsilon_{eq} \approx 20$ where a high degree of strain hardening is observed before reaching the hardness satura-

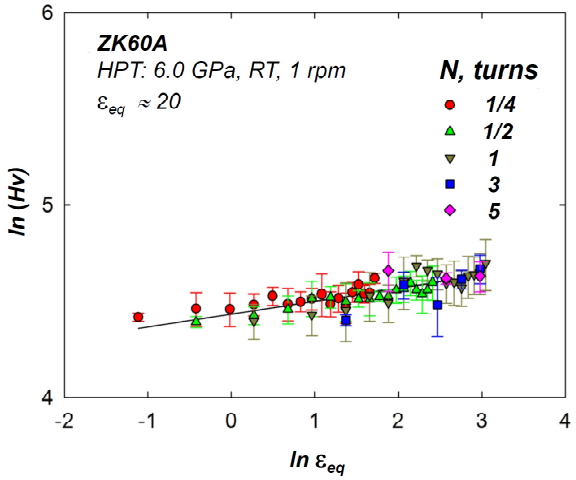

Fig. 6. A double-natural logarithmic plot of the measured *Hv* values versus ε_{eq} for the ZK60A alloy after HPT for up to 5 turns under an applied pressure of 6.0 GPa where the plot covers data up to $\varepsilon_{eq} \approx 20$ and the error bars show the 95% confidence level, adapted from our work [41].

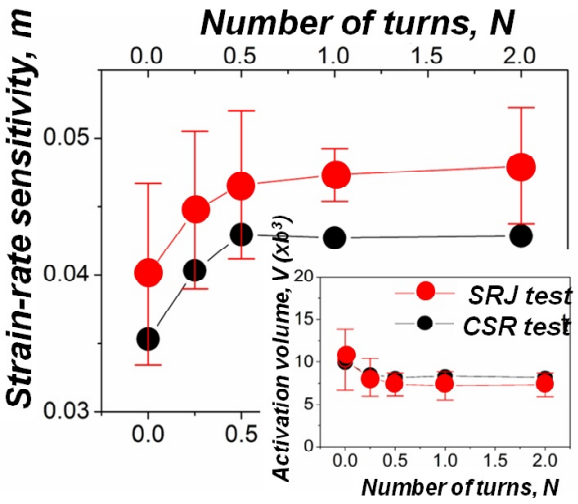

Fig. 7. Variations of the strain rate sensitivity with different levels of torsion straining: datum points are shown for CSR and SRJ testing, adapted from our work [32].

tion [41]. The solid line in Fig. 6 describes the trend of all datum points which denotes the following form:

$$Hv = 84\,\varepsilon_{eq}^{0.07}. \quad (4)$$

Thus, a high level of strain hardening with $\eta \approx 0.07$ was recorded in the early stage of HPT processing for the ZK60A alloy where a positive exponent denotes strain hardening. This result is consistent with the value of $\eta \approx 0.08$ for an AZ31 magnesium alloy after HPT for 1 and 5 turns at 6.0 GPa [41] and these Mg alloys demonstrate a stronger strain hardening behavior than the processed Ti alloy reported earlier [42].

For UFG materials after SPD, the measured ductility is always an issue due to the essential character described by the paradox of strength and ductility where UFG materials generally exhibit high strength but very limited ductility at RT [43-45]. Accordingly, micro-mechanical behavior was evaluated for the UFG ZK60A alloy after HPT by applying a novel nanoindentation technique.

The nanoindentation tests were conducted on the initial as-extruded sample and on the disk edges of the ZK60A alloy after HPT up to 2 turns at four different indentation strain rates from 0.0125 to 0.1 s^{-1} using two different indentation procedures: constant strain rate (CSR) testing and strain-rate jump (SRJ) testing. These two separate procedures were performed by utilizing a three-sided pyramidal Berkovich indenter for estimating the strain rate sensitivity, *m*, where the *m* values are determined by following the earlier procedures and applying the measured hardness, *H*, through nanoindentation [46]. The results are summarized in Fig. 7 where *N* = 0 denotes the as-extruded condition and the estimated *m* values are plotted with increasing numbers of turns [32]. It should be noted that the essential merit of the SRJ test is that the estimation is conducted from a single indentation whereas multiple indentations are required in the CSR tests.

There is an overall consistency in the trend of the *m* values with increasing numbers of HPT turns for these two testing methods through the nanoindentation analysis although slight differences are recorded in the *m* values such as ~0.048 from SRJ and ~0.043 from CSR after HPT for 2 turns. Thus, the *m* value of ~0.035-0.040 in the initial condition prior to HPT was enhanced significantly to *m* H" 0.043-0.047 after HPT for 1/2 turn and thereafter the values remain reasonably constant through 2 turns. Thus, the examination through nanoindentation showed that the UFG Mg alloy demonstrated a high potential for exhibiting an improved plasticity at RT after HPT even after successful microstructural refinement leading to high hardness. A very recent review summarized the nano- and micro-mechanical properties of UFG materials after SPD [47] and a comprehensive tabulation of avail-

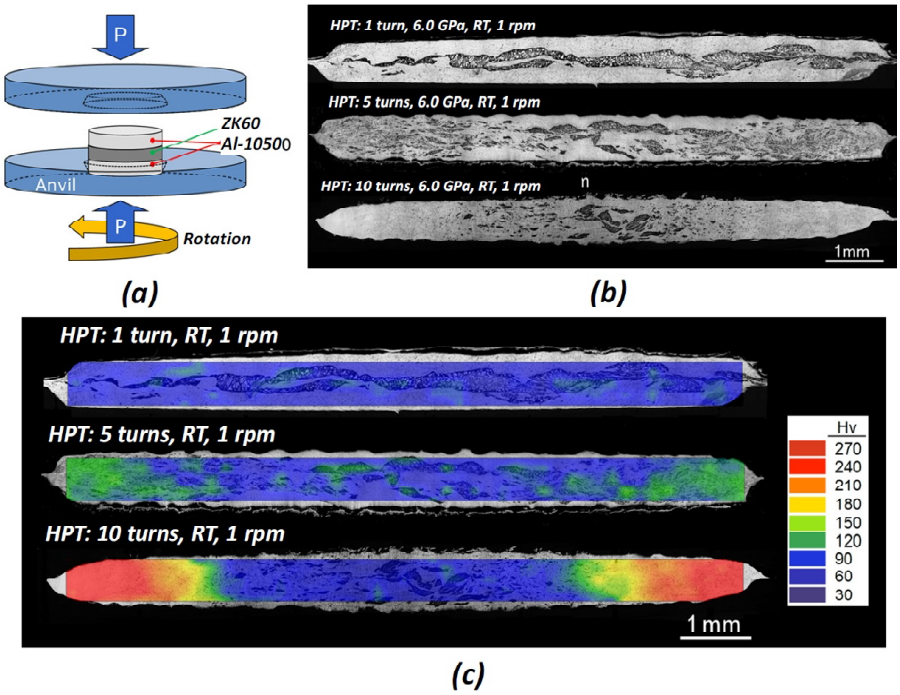

Fig. 8. (a) Schematic illustration of the sample set-up for HPT processing using three different disks and (b) an overview of the microstructures after processing through 1, 5 and 10 turns and (c) color-coded hardness contour maps taken at the vertical cross-sections along the disk diameters after HPT for 1, 5 and 10 turns, adapted from our works [57-59].

able experimental data was presented which demonstrated that an enhancement in ductility of UFG metals at RT is anticipated by the sustained plasticity by activating different flow mechanisms such as grain boundary sliding. This accounts for the increase in the *m* value with the increasing amount of straining by SPD.

3. SYNTHESIS OF AN EXTRA HARD HYBRID METAL BY HPT PROCESSING

Processing by HPT generally provides the potential for achieving high hardness in most bulk metals due to significant grain refinement. In recent years, because of the introduction of intense plastic strain during processing, HPT has also been applied for the consolidation of metallic powders [48-54] and the bonding of machining chips [55,56]. Applying the conventional processing of HPT, it is anticipated that it may be possible to produce a new metal system from a combination of simple dissimilar metal solids and, in addition, the metal system may exhibit superior mechanical properties which are above the upper limits of the properties that these individual base metals can achieve through SPD. Accordingly, a new approach for the formation of an Al-Mg hybrid system was demonstrated by processing two commercial metal disks of the Al-1050 and ZK60 alloys through HPT and Figs. 8 and 9 show the unique microstructure and hardness distributions and a detailed analysis of the strengthening mechanism, respectively, for the Al-Mg hybrid system formed by HPT [57-59].

This experiment used commercial Al-1050 and ZK60A alloys where these alloys are very similar or consistent alloys as described in the earlier sections. The disks of these alloys were prepared using the regular procedure and conventional HPT processing was conducted at RT under quasi-constrained conditions. In particular, two separate disks of the Al and Mg alloys were piled up with the order of Al/Mg/Al where the Mg disk was placed between two Al disks without placing any glue or using any metal brushing treatment as shown in Fig. 8(a) [57,58]. Then, a set of the piled up disks was processed by HPT at RT under 6.0 GPa for totals of 1, 5 and 10 turns at a constant rotational speed of 1 rpm.

An overview of the microstructure was obtained using an optical microscope at the vertical cross-sections along the disk diameters after HPT processing followed by polishing and chemically etch-

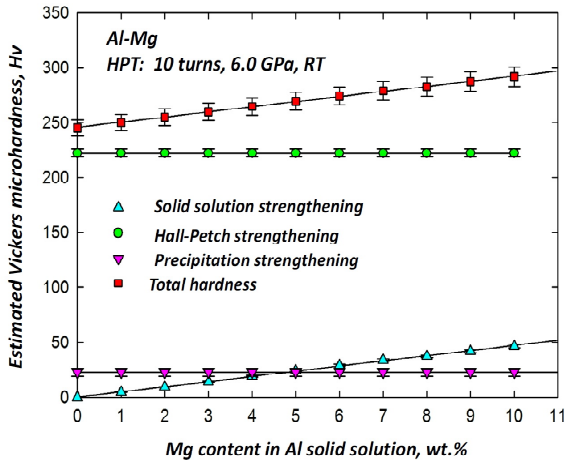

Fig. 9. Estimated Vickers microhardness values with increasing Mg content in Al solid solutions in disks processed by HPT for 10 turns, adapted from our works [57].

ing and the micrographs are shown for 1, 5 and 10 turns from the top, respectively, in Fig. 8b [57-59]. As is apparent in Fig. 8b, a multi-layered structure with fragmented Mg layers with thicknesses of ~200 μm appearing in a dark color was visible in the Al matrix appearing in a bright color without any segregation throughout the disk after 1 turn and in the central region at r <2.0 and <1.0 mm of the disks after 5 and 10 turns, respectively. However, the disk edge at r >2.5 mm after 5 turns demonstrated a unique microstructure where there is a homogeneous distribution of very fine Mg phases with thicknesses of ~5-10 μm to even a true nano-scale of ~100-500 nm within an Al matrix. Moreover, there were no visible Mg phases at the disk edge at ~3< r <5 mm after 10 turns.

Detailed microstructural analysis through TEM showed that a true nanostructure was formed with spatial grain sizes of ~190 nm and ~90 nm at the disk edges after 5 and 10 turns, respectively [57]. A detailed chemical analysis by energy-dispersive X-ray spectroscopy (EDS) in a scanning transmission electron microscope (STEM) observed a small volume with <5 vol.% of an irregularly-distributed intermetallic compound, γ-Al_3Mg_2, as a form of thin layers of ~20 nm and ~30 nm in the Al matrix after 5 and 10 turns, respectively. In addition, a high resolution TEM analysis and an X-ray diffraction (XRD) analysis using Materials Analysis Using Diffraction (MAUD) software revealed the formation of another intermetallic compound of γ-$Al_{12}Mg_{17}$ in the Al matrix where this is within the matrix in a supersaturated solid solution state at the disk edge after 10 turns due to rapid diffusion of Mg from the fine Mg-rich phases which are visible after 5 turns of HPT. Thus, the simultaneous processing by HPT of the Al and Mg disks synthesizes an intermetallic-based Al metal matrix nanocomposite (MMNC) in the highly deformed region around the peripheries of the disks after HPT.

Subsequently, the distribution of Vickers microhardness was examined over the vertical cross-sections of the processed disks and the data set was visualized by constructing color-coded hardness contour maps as shown in Fig. 8c for 1, 5 and 10 turns from the top, respectively, where the hardness values are indicated in the key on the right. For reference, the initial values of Hv were ~65 for the Al-1050 alloy [60] and ~110 for the ZK60 alloy as shown in Fig. 5 after HPT for 5 turns and these Hv values reached a saturation level across the disk diameters through sufficient torsional straining.

The total cross-section after HPT for 1 turn shows an average microhardness value of ~70 which is similar to the value of ~65 for the base material of the Al-1050 alloy after HPT for 5 turns and this value remains constant at the centers at r <2.5 mm of the Al-Mg disks up to 10 turns. However, high hardness with a maximum of $Hv \approx 130$ was achieved in the peripheral region after 5 turns where the fine Mg phase is homogeneously distributed within the Al matrix. There is a significant increase in Hv after 10 turns where a maximum hardness of ~270 was recorded at the peripheral region at r >3.0 mm. The high hardness values of the Al-Mg system after HPT are much higher than the HPT-processed base alloys of Al and Mg and thus these results demonstrate that the formation of intermetallic compounds leading to the synthesis of MMNC may provide the possibility of improving the upper limit on the maximum hardness value in the hybrid Al-Mg system through HPT processing.

The major strengthening mechanisms were evaluated for achieving exceptional hardness in the intermetallic-based MMNC synthesized by HPT for 5 and 10 turns under 6.0 GPa at RT. Thus, the achievable Vickers microhardness value was estimated by the sum of the separate strengthening mechanisms expressed by Hall-Petch strengthening due to significant grain refinement, solid solution strengthening because of the high content of Mg atoms leading to the increased frictional stress within the crystal lattices, and precipitation hardening by the thin layers of the β-Al_3Mg_2 intermetallic compound. The estimated total hardness is shown in Fig. 9 with increasing Mg content in an Al solid so-

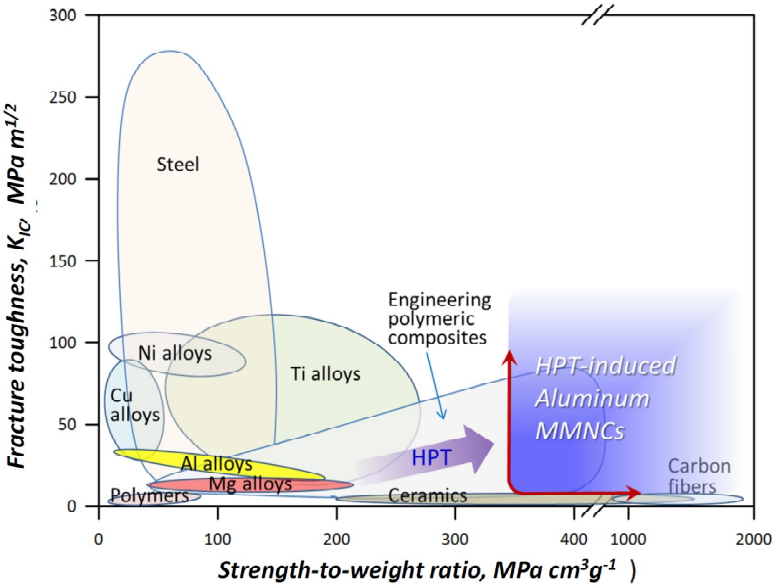

Fig. 10. The range of fracture toughness and strength-to-weight ratio for many metals and materials [66] where the synthesized Al–Mg system after HPT is incorporated as the region of HPT-induced aluminum MMNC without delineating any upper limits, adapted from our works [59].

lution matrix in the disk after HPT for 10 turns [57]. Since the synthesized MMNC after 10 turns contained very small volumes of intermetallic compounds in the form of thin layers, Hall-Petch strengthening by grain refinement was anticipated to provide the highest contribution to the total hardness whereas there was an increasing contribution of solution strengthening with increasing Mg contents in the Al matrix. This estimate was in excellent agreement with the experimental values of hardness in the synthesized Al-Mg alloy after HPT, thereby confirming the simultaneous occurrence of these separate strengthening mechanisms which is a consequence of the low processing temperature and the short operating time which prevents the occurrence of any significant microstructural recovery. It should be noted that the rapid diffusivity of Mg atoms into the Al matrix is a key process for the diffusion bonding of Al and Mg though HPT and a recent review describes the significance of the fast atomic mobility during SPD by recognizing the significant increase in the vacancy concentration through SPD processing [61].

4. FUTURE POTENTIAL FOR HPT PROCESSING

Extensive investigations have been attempted to improve the physical and mechanical properties of metals and materials by grain refinement through the application of SPD. In particular, research in the last decade has demonstrated that SPD processing is also feasible for the production of unusual phase transformations and in the introduction of a range of nanostructural features [62,63]. Therefore, not only improving hardness, strength and ductility of a single material as demonstrated earlier for the Al-3% Mg and ZK60 alloys but also processing by SPD can be developed for the alternative approach of introducing high performance materials through diffusion bonding of dissimilar metals. This is achieved by synthesizing new metal systems and ultimately producing MMNCs as demonstrated for the bonding of Al and Mg alloys through HPT. There are at present only a limited number of reports demonstrating a sold-state reaction in an Al-Cu system through the bonding of semicircular half-disks of Al and Cu through HPT at ambient temperature through 100 turns [64] and a vision of architecturing hybrid metals through HPT by computational calculations [65].

Considering the future potential of the hybrid materials processed by SPD, it is reasonable to visualize an enhancement in the specific strength of the MMNC synthesized at the disk edges of the Al-Mg system by comparison with the base metals of Al and Mg alloys and some other engineering materials. Fig. 10 shows a toughness-strength diagram reported earlier and delineating the range of fracture toughness and strength-to-weight ratio for

many metals and materials [66]. Assuming a general similarity in the trends of plasticity and toughness of materials [67], the synthesized Al-Mg system after HPT is now incorporated into the diagram without delineating any upper limits [59]. The border line for the field of the Al-Mg system was applied with the extraordinary strength of the hybrid Al-Mg system after 10 HPT turns demonstrating an excellent strength-to-weight ratio of ~350 MPa·cm^{3}·g^{-1} under a measured density of 2.48 g·cm^{-3} and the recorded hardness of $Hv \approx 270$ which is equivalent to ~865 MPa in tensile strength. Thus, the strength-to-weight ratio of the Al-Mg system after HPT is anticipated to be much higher than many steels and Ti alloys and it may even be similar to some strong engineering polymeric composites.

Finally, it should be emphasized that the bulk materials produced through the HPT processing of separate disks may contain a gradient-type microstructure [68-70] or a heterogeneous nanostructure [71] according to grain size and composition [57-59,72] as was seen in the radial direction from the centers of the HPT disks in Figs. 8b and 8c. A recent report defined this kind of new materials organization as *heterogeneous architecture materials* [73]. Although this type of microstructure is common in many biological systems [74,75], it is a new category of structure in engineering materials and it is expected to lead to a significant potential for exhibiting excellent mechanical properties.

5. SUMMARY AND CONCLUSIONS

1. This report demonstrates the successful HPT processing of an Al-3% Mg alloy and a ZK60A magnesium alloy leading to significant grain refinement and high hardness. These two alloys demonstrate a common strain hardening behavior such that there is a hardness evolution towards homogeneity with a saturated high hardness after larger numbers of HPT revolutions.
2. Conventional HPT processing was applied successfully for the synthesis of a hybrid Al-Mg alloy system having a unique microstructural distribution within the disk through the diffusion bonding of separate Al and Mg alloy disks. A unique microstructure was observed with an Al-Mg multilayered structure at the disk center and with a metal matrix nanocomposite at the disk edge after processing through 5-10 turns.
3. An excellent description of Hall-Petch strengthening was demonstrated in the Al-3% Mg alloy through the grain size reduction. The exceptional hardness in the MMNC at the Al-Mg disk edge was verified as a consequence of Hall-Petch strengthening having the highest contribution whereas solid solution strengthening and precipitation hardening contributed simultaneously with relatively minor contributions.
4. It is concluded that there is an excellent potential for making use of HPT processing in introducing new alloy systems from different metals and in developing unique materials having gradient or heterogeneous microstructures. Further investigations are now needed to fully exploit this new approach.

ACKNOWLEDGEMENTS

This work was supported by the NRF Korea funded by MoE under Grant No. NRF-2014R1A1A2057697 and NRF-2016R1A6A1A03013422, and by MSIP under Grant No. NRF-2016K1A4A3914691 (MK); the NRF Korea funded by MSIP under Grant No. NRF-2014M2A8A1030385 (JIJ); and the European Research Council under ERC Grant Agreement No. 267464-SPDMETALS (TGL).

REFERENCES

[1] E.O. Hall // *Proc. Phys. Soc. B* **64** (1951) 747.
[2] N.J. Petch // *J. Iron Steel Inst.* **174** (1953) 25.
[3] R.W. Armstrong // *Metall. Mater. Trans. A* **47A** (2016) 5801.
[4] N. Balasubramanian and T.G. Langdon // *Metall. Mater. Trans. A* **47A** (2016) 5827.
[5] R.Z. Valiev, R.K. Islamgaliev and I.V. Alexandrov // *Prog. Mater. Sci.* **45** (2000) 103.
[6] R.Z. Valiev and T.G. Langdon // *Prog. Mater. Sci.* **51** (2006) 881.
[7] A.P. Zhilyaev and T.G. Langdon // *Prog. Mater. Sci.* **53** (2008) 893.
[8] A.P. Zhilyaev, B.K. Kim, G.V. Nurislamova, M.D. Baró, J.A. Szpunar and T.G. Langdon // *Scripta Mater*. **46** (2002) 575.
[9] A.P. Zhilyaev, G.V. Nurislamova, B.K. Kim, M.D. Baró, J.A. Szpunar and T.G. Langdon // *Acta Mater*. **51** (2003) 753.
[10] J. Wongsa-Ngam, M. Kawasaki and T.G. Langdon // *J. Mater. Sci.* **48** (2013) 4653.
[11] R.Z. Valiev, Yu.V. Ivanisenko, E.F. Rauch and B. Baudelet // *Acta Mater.* **44** (1996) 4705.
[12] R.B. Figueiredo, P.R. Cetlin and T.G. Langdon // *Mater. Sci. Eng. A* **528** (2011) 8198.
[13] H.-J. Lee, J.-K. Han, S. Janakiraman, B. Ahn, M. Kawasaki and T.G. Langdon // *J. Alloys Compds* **686** (2016) 998.

[14] A. Hohenwarter, A. Bachmaier, B. Gludovatz, S. Scheriau and R. Pippan // *Int. J. Mat. Res.* **100** (2009) 12.
[15] M. Kawasaki, R.B. Figueiredo and T.G. Langdon // *Acta Mater.* **59** (2011) 308.
[16] M. Kawasaki, R.B. Figueiredo and T.G. Langdon // *J. Mater. Sci*. **47** (2012) 7719.
[17] M. Kawasaki, R.B. Figueiredo, Y. Huang and T.G. Langdon // *J. Mater. Sci*. **49** (2014) 6586.
[18] M. Kawasaki // *J. Mater. Sci*. **49** (2014) 18.
[19] R.Z. Valiev, F. Chmelik, F. Bordeaux, G. Kapelski and B. Baudelet // *Scripta Metall. Mater.* **27** (1992) 855.
[20] Y. Ma, Z. Horita, M. Furukawa, M. Nemoto, R.Z. Valiev and T.G. Langdon // *Mater. Lett.* **23** (1995) 283.
[21] M. Furukawa, Z. Horita, M. Nemoto, R.Z. Valiev and T.G. Langdon // *Acta Mater.* **44** (1996) 4619.
[22] G. Sakai, Z. Horita and T.G. Langdon // *Mater. Sci. Eng. A* **393** (2005) 344.
[23] Z. Horita and T.G. Langdon // *Mater. Sci. Eng. A* **410-411** (2005) 422.
[24] S.V. Dobatkin, V.V. Zakharov, A.Yu. Vinogradov, K. Kitagawa, N.A. Krasil'nikov, T.D. Rostova and E.N. Bastarash // *Russ. Metall.* **2006** (2006) 533.
[25] A.A. Mazilkin, B.B. Straumal, E. Rabkin, B. Baretzky, S. Enders, S.G. Protasova, O.A. Kogtenkova and R.Z. Valiev // *Acta Mater*. **54** (2006) 3933.
[26] R.Z. Valiev, N.A. Enikeev, M.Yu. Murashkin, V.U. Kazykhanov and X. Sauvage // *Scripta Mater*. **63** (2010) 949.
[27] X. Sauvage, N. Enikeev, R. Valiev, Y. Nasedkina and M. Murashkin // *Acta Mater.* **72** (2014) 125.
[28] O. Andreau, J. Gubicza, N.X. Zhang, Y. Huang, P. Jenei and T.G. Langdon // *Mater. Sci. Eng. A* **615** (2014) 231.
[29] P. Bazarnik, Y. Huang, M. Lewandowska and T.G. Langdon // *Mater. Sci. Eng. A* **626** (2015) 9.
[30] M. Furukawa, Z. Horita, M. Nemoto, R.Z. Valiev and T.G. Langdon // *Philos. Mag. A* **78** (1998) 203.
[31] T.G. Langdon // *Acta Mater*. **61** (2013) 7035.
[32] I.C. Choi, D.H. Lee, B. Ahn, K. Durst, M. Kawasaki, T.G. Langdon and J.I. Jang // Scripta Mater. **94** (2015) 44.
[33] R.B. Figueiredo and T.G. Langdon // *Mater. Sci. Eng. A* **501** (2009) 105.
[34] S.A. Torbati-Sarraf and T.G. Langdon // *J. Alloy Compds* **613** (2014) 357.
[35] R.B. Figueiredo and T.G. Langdon // *J. Mater. Sci.* **45** (2010) 4827.
[36] A. Vorhauer and R. Pippan // *Scripta Mater.* **51** (2004) 921.
[37] K. Edalati, J.M. Cubero-Sesin, A. Alhamidi, I.F. Mohamed and Z. Horita // *Mater. Sci. Eng. A* **613** (2014) 103.
[38] C. Xu, Z. Horita and T.G. Langdon // *Acta Mater*. **55** (2007) 203.
[39] K. Edalati, Y. Ito, K. Suehiro and Z. Horita // *Int. J. Mater. Res*. **100** (2009) 1668.
[40] M. Kawasaki, B. Ahn and T.G. Langdon // *Mater. Sci. Eng. A* **527** (2010) 7008.
[41] H.-J. Lee, S.K. Lee, K.H. Jung, G.A. Lee, B. Ahn, M. Kawasaki and T.G. Langdon // *Mater. Sci. Eng. A* **630** (2015) 90.
[42] Y.C. Wang and T.G. Langdon // *J. Mater. Sci.* **48** (2013) 4646.
[43] R.Z. Valiev, I.V. Alexandrov, Y.T. Zhu and T.C. Lowe // *J. Mater. Res.* **17** (2002) 5.
[44] R. Valiev // *Nature* **419** (2002) 887.
[45] R. Valiev // *Nature Mater*. **3** (2004) 511.
[46] I.-C. Choi, Y.-J. Kim, Y.M. Wang, U. Ramamurty and J.-I. Jang // *Acta Mater.* **61** (2013) 7313.
[47] M. Kawasaki, B. Ahn, P. Kumar, J.I. Jang and T.G. Langdon // *Adv. Eng. Mater.* (in press) DOI: 10.1002/adem.201600578
[48] A.V. Korznikov, I.M. Safarov, D.V. Laptionok and R.Z. Valiev // *Acta Metall. Mater*. **39** (1991) 3193.
[49] V.V. Stolyarov, Y.T. Zhu, T.C. Lowe, R.K. Islamgaliev and R.Z. Valiev // *Mater. Sci. Eng. A* **282** (2000) 78.
[50] K. Edalati, Z. Horita, H. Fujiwara and K. Ameyama // *Metall. Mater. Trans. A* **41A** (2010) 3308.
[51] M. Ashida, Z. Horita, T. Kita and A. Kato // *Mater. Trans*. **53** (2012) 13.
[52] J.M. Cubero-Sesin and Z. Horita // *Mater. Sci. Eng. A* **558** (2012) 462.
[53] K. Edalati, S. Toh, H. Iwaoka and Z. Horita // *Acta Mater*. **60** (2012) 3885.
[54] K. Edalati, T. Daio, Z. Horita, K. Kishida and H. Inui // *J. Alloys Compds* **563** (2013) 221.
[55] A.P. Zhilyaev, A.A. Gimazov, G.I. Raab and T.G. Langdon// *Mater. Sci. Eng. A* **486** (2008) 123.
[56] K. Edalati, Y. Yokoyama and Z. Horita // *Mater. Trans.* **51** (2010) 23.

[57] B. Ahn, A.P. Zhilyaev, H.-J. Lee, M. Kawasaki and T.G. Langdon // *Mater. Sci. Eng. A* **635** (2015) 109.
[58] M. Kawasaki, B. Ahn, H.-J. Lee, A.P. Zhilyaev and T.G. Langdon // *J. Mater. Res*. **31** (2016) 88.
[59] B. Ahn, H.-J. Lee, I.C. Choi, M. Kawasaki, J.I. Jang and T.G. Langdon // *Adv. Eng. Mater.* **18** (2016) 1001.
[60] M. Kawasaki, S.N. Alhajeri, C. Xu and T.G. Langdon // *Mater. Sci. Eng. A* **529** (2011) 345.
[61] X. Sauvage, G. Wilde, S.V. Divinski, Z. Horita and R.Z. Valiev // *Mater. Sci. Eng. A* **540** (2012) 1.
[62] R.Z. Valiev, Y. Estrin, Z. Horita, T.G. Langdon, M.J. Zehetbauer and Y. Zhu // *JOM* **68** (2016) 1216.
[63] R.Z. Valiev, Y. Estrin, Z. Horita, T.G. Langdon, M.J. Zehetbauer and Y.T. Zhu // *Mater. Res. Lett.* **4** (2016) 1.
[64] K. Oh-ishi, K. Edalati, H.S. Kim, K. Hono and Z. Horita // *Acta Mater*. **61** (2012) 3482.
[65] O. Bouaziz, H.S. Kim and Y. Estrin // *Adv. Eng. Mater*. **15** (2013) 336.
[66] K. Lu // *Science* **328** (2010) 319.
[67] M.F. Ashby, *Materials Selection in Mechanical Design* (Butterworth-Heinemann, Oxford, U.K., 2005).
[68] T.H. Fang, W.L. Li, N.R. Tao and K. Lu // *Science* **331** (2011) 1587.
[69] X. Wu, P. Jiang, L. Chen, F. Yuan and Y.T. Zhu // *Proc. Natl. Acad. Sci.* **111** (2014) 7197.
[70] K. Lu // *Science* **345** (2014) 1455.
[71] X.L. Wu, P. Jiang, L. Chen, J.F. Zhang, F.P. Yuan and Y.T. Zhu // *Mater. Res. Lett.* **2** (2014) 185.
[72] J.Y. Kang, J.G. Kim, H.W. Park and H.S. Kim // *Sci. Rep.* **6** (2016) 26590/1.
[73] O. Bouaziz, Y. Bréchet and J.D. Embury // *Adv. Eng. Mater*. **10** (2008) 24.
[74] M.A. Meyers, P.-Y. Chen, A.Y.-M. Lin and Y. Seki // *Prog. Mater. Sci.* **53** (2008) 1.
[75] P.-Y. Chen, J. McKittrick and M.A. Meyers // *Prog. Mater. Sci.* **57** (2012) 1492.